Growth of carbon nanotubes inside boron nitride nanotubes by coalescence of fullerenes: towards the world's smallest co-axial cable

Kate E. Walker, Graham A. Rance,* Áron Pekker, Hajnalka M. Tóháti, Michael W. Fay, Rhys W. Lodge, Craig T. Stoppiello, Katalin Kamarás, Andrei N. Khlobystov*

K. E. Walker, R. W. Lodge, Dr. C. T. Stoppiello, Prof. A. N. Khlobystov

School of Chemistry, University of Nottingham, University Park, Nottingham, NG7 2RD, UK.

E-mail: Andrei.Khlobystov@nottingham.ac.uk

Dr. G. A. Rance, Dr. M. W. Fay

Nanoscale and Microscale Research Centre, Cripps South, University of Nottingham,

University Park, Nottingham, NG7 2RD, UK.

E-mail: Graham.Rance@nottingham.ac.uk

Dr. Á. Pekker, H. M. Tóháti, Prof. K. Kamarás

Institute for Solid State Physics and Optics, Wigner Research Centre for Physics, Hungarian

Academy of Sciences, Konkoly-Thege M. 29-33, 1121 Budapest, Hungary.

The use of boron nitride nanotubes as effective nanoscale containers for the confinement and thermal transformations of molecules of C_{60}-fullerene has been demonstrated. The gas-phase insertion of fullerenes into the internal channel of boron nitride nanotubes yields quasi-one-dimensional arrays, with packing arrangements of the guest-fullerenes different to those in the

1

bulk crystal and critically dependent on the internal diameter of the host-nanotube. Interestingly, the confined fullerene molecules (i) exhibit dynamic behaviour and temperature-dependant phase transitions analogous to that observed in the bulk crystal and (ii) can be effectively removed from within the internal channel of nanotubes by excessive sonication in organic solvent, indicating weak host-guest interactions. The thermal treatment of fullerenes confined within nanotubes at 1200 °C in argon triggers the polymerisation and coalescence of the guest-fullerenes into carbon nanotubes inside boron nitride nanotubes affording a hybrid nanostructure – the world's smallest coaxial cable – on a preparative scale, as confirmed by high resolution bright field transmission electron microscopy (TEM) imaging and electron energy loss spectroscopy, energy filtered transmission electron microscopy (EELS, EFTEM) elemental mapping and UV-vis absorption spectroscopy.

1. Introduction

Carbon nanotubes (CNTs) are hollow, one-dimensional containers, with high tensile strength,[1] chemical stability[2] and electrical conductivity.[3] Described as the world's smallest test tube, they behave as excellent nanoscale containers for molecules,[4-6] metals[7-9] and metal halides,[10] where the spontaneous encapsulation is driven by van der Waals forces that stabilise the confined guest-species in the internal channel of the host-nanotube.[11] Moreover, a good geometric fit between the critical dimensions of the encapsulated guest and the internal dimensions of the host can result in van der Waals forces that are sufficiently high that insertion is irreversible. This effective nanoscale confinement permits the study of the structure,[12-13] motion[14] and dynamics[15-16] of individual molecules.

Furthermore, extreme spatial confinement in CNTs allows us to probe the kinetics and pathways of chemical reactions and processes at the nanoscale, including the formation of

one-dimensional materials templated by the internal channel of the host-nanotube.[6, 17-18] The simplest and most widely studied confined transformation in single-walled carbon nanotubes (SWCNTs) is the conversion of C_{60}@SWCNT, so-called 'peapods', into double-walled carbon nanotubes (DWCNTs) *via* the thermally activated polymerisation and coalescence of guest-fullerenes to an internal carbon nanotube.[17,19] Numerous more complex processes have also been observed inside nanotubes, such as unusual oligomerisation and polymerisation reactions,[13, 20-21] the growth of graphene nanoribbons[22-24] and the formation of molecular nanodiamonds[18] from encapsulated fullerenes and organic molecules respectively. As such, chemical reactions inside carbon nanotubes open up new avenues for the synthesis of nanoscale materials with unique structures and functional properties inaccessible by other means.

Boron nitride nanotubes (BNNTs) are isoelectronic to CNTs and similarly possess high mechanical strength[25] and excellent chemical and thermal stabilities.[26] In contrast to CNTs, however, BNNTs are electronically insulating, a consequence of the partly ionic interatomic B-N bonding, and optically transparent with a wide bandgap.[27-28] Whilst less well explored relative to CNTs, BNNTs represent a remarkable class of one-dimensional nanoscale containers for metals,[29-34] metal halides[35-36] and molecules, such as C_{60},[37] and owing to their transparency to visible light offer the opportunity to probe the photochemistry of encapsulated molecules. Like CNTs, the encapsulation of guest-species into BNNTs is modulated by ubiquitous van der Waals forces between host and guest.[38] Yet, as the polarity of interatomic bonding, delocalisation of π electrons and polarisability differ significantly between CNTs and BNNTs, the extent to which these properties can influence the interactions between BNNTs and molecules are at present not fully understood. Moreover, experimental studies on the structure, motion, dynamics and reactivity of molecules in BNNTs are still

extremely limited, particularly those that afford hybrid nanostructures on the preparative scale, with one rare example being the formation of metal particles from metal halides.[36]

In this study, we make the first important steps towards establishing BNNTs as a nanoreactor through the thermally-assisted polymerisation and coalescence of C_{60}, a classical model reaction in CNTs, as a test reaction for BNNT nanoreactors. The interactions of C_{60} with BNNTs and intermolecular reactions of C_{60} inside the nanotube demonstrates the ability of BNNTs to act as an effective template of one-dimensional nanostructures, ultimately leading to the formation of CNT@BNNT, where an electrically conducting CNT is embedded within an insulating BNNT. Such a nanostructure – the world's smallest co-axial cable – affordable using our approach on a preparative scale is predicted to have a wealth of unique functional properties for applications in nanoelectronics and sensing devices.[39-41]

2. Results and Discussion

A fundamental requirement for the transfer of any guest-species into the inner cavity of a host-nanotube is the presence of accessible holes through which the guests can pass. Our TEM observations (see Supporting Information, Figure S1) indicate that whilst the internal diameter of BNNTs ($d_{int} = 2.45\pm1.19$ nm) is large enough to accommodate C_{60} (van der Waals diameter $d_{vdW} = 1.0$ nm), most nanotubes are capped and possess a moderate amount of boron-containing impurities which will prohibit the transport of C_{60} into the inner channel. Therefore, the first challenge in our multi-step synthetic strategy (Figure 1) was to develop a reliable method for opening and purifying BNNTs.
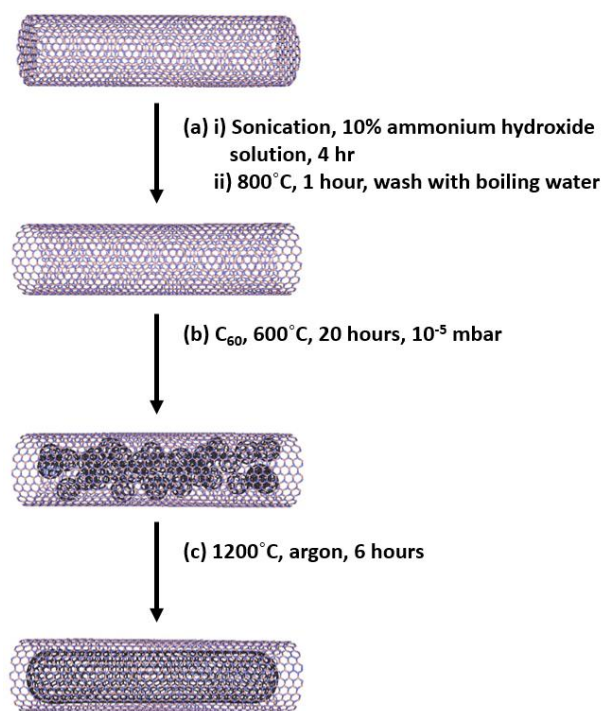
Figure 1. The multi-step method used to produce CNT@BNNT: (a) the opening and purification of BNNTs, (b) the encapsulation of C_{60} into BNNTs and (c) the transformation of C_{60} to CNTs in BNNTs.

A variety of different methods have been reported for the selective opening of BNNTs.[42-45] We have tested (i) oxidation in air (Method 1), (ii) ball milling (Method 2) and (iii) hydrolysis followed by oxidation in air (Method 3a-c) for the controlled opening and purification of BNNTs, and found Method 3a to be the most effective (Table 1 and Supporting Information, Figure S2, S3 and S4).

Table 1. Comparison of methods for opening and purifying BNNTs.

Method	Conditions	LNT / μm [a]	% open [a]	B : N [b]
-	as-received	> 200	< 1	61 : 39
1	oxidation in air (800 ℃, 1 hr)	> 200	< 1	87 : 13
2	ball milling (10 Hz, 90 min)	1.98 ± 0.78	80	57 : 43
3a	hydrolysis (4 hr), oxidation in air (800 ℃, 1 hr)	0.55 ± 0.22	83	51 : 49
3b	hydrolysis (10 hr), oxidation in air (800 ℃, 1 hr)	0.16 ± 0.05	81	55 : 45
3c	hydrolysis (24 hr), oxidation in air (800 ℃, 1 hr)	0.14 ± 0.06	88	55 : 45

[a] Determined by statistical analysis of TEM images; [b] Determined by EDX spectroscopy.

In Method 3, the lone pair of electrons on the N atom of the ammonia molecules interact with the empty p_z orbital of B in the as-received BNNTs, activating B-N bonds towards hydrolysis and causing the corrosion, thinning and removal of the BNNT end-caps. The end-caps typically contain strained four- or eight- membered rings,[46,47] making them more susceptible to reaction with water molecules than the less strained six-membered rings forming the sidewalls and thus are selectively removed. The resultant BNNTs are terminated with either ammonia, or hydroxyl groups as a result of hydrolysis, causing them to be more hydrophilic and dispersible in water. A significant reduction in the mean length from over 200 μm to 0.55±0.22 μm, essential for minimisation of the expected length-dependent transport resistance of guest-molecules within the host-nanotube,[48] as measured by TEM was determined through statistical analysis of multiple micrographs, and the resulting BNNTs are free of the boron impurities as confirmed by EDX spectroscopy. Most importantly, the BNNTs subsequent to this treatment are open, as well as shorter and purer, making them suitable for filling with guest-molecules.

The encapsulation of C_{60} into BNNTs was carried out at 600 °C in vacuum which is based on an effective method for the preparation of C_{60}@CNT.[12] The encapsulation of C_{60} into CNTs is known to be a highly exothermic and generally irreversible process (up to 3 eV per C_{60}, depending on the specific van der Waals contact area between the convex external surface of C_{60} and the concave internal surface of the CNT channel),[49,50] in which adsorbed C_{60} migrates along the surface of the CNT before entering at the termini and at accessible defect sites along the sidewall. Provided the CNT diameter is large enough to accommodate C_{60} molecules (0.6 nm wider than the diameter of the guest molecule), the CNTs will be completely filled.[12, 51, 52] Whilst the encapsulation of C_{60} into BNNTs has been reported,[37] no experimental studies to date report the energy of encapsulation of C_{60} into BNNTs. However, the calculated energy of adsorption for C_{60} onto graphene (0.85 eV) is comparable to C_{60} onto hexagonal boron nitride sheets (0.83 eV),[50] suggesting similar interactions for C_{60}@BNNT and C_{60}@CNT.[53] Moreover, the calculated energy for encapsulation into CNTs and BNNTs suggests that the energy gain for the insertion of C_{60} into BNNTs (C_{60}@(10, 10)BNNT ΔE = 4.38 eV) may surpass that of the CNT analogue (C_{60}@(10, 10)CNT ΔE = 3.02 eV).[38]

TEM imaging confirms the filling of BNNTs under our conditions (Figure 2). Similarly to CNTs with internal diameters matching the van der Waals diameter of C_{60}, the guest-molecules of C_{60} confined within narrow BNNTs line up in a single-chain, with separations of *ca*. 0.3 nm between the neighbouring fullerenes and between the fullerene and the internal walls of BNNTs (Figure 2a). The inter-fullerene distance is *ca*. 0.9-1.0 nm (depending on the diameter of the host-nanotube), consistent with a previous study of C_{60} in BNNTs[37] and the minimum separation in the bulk fcc-crystal (1.0 nm)[54, 55] and slightly smaller than in SWCNTs (1.1 nm)[48] as a result of tighter packing arrangements. These

measurements indicate that the nature of C_{60}-BNNT interactions is similar to that of C_{60}-CNT interactions.
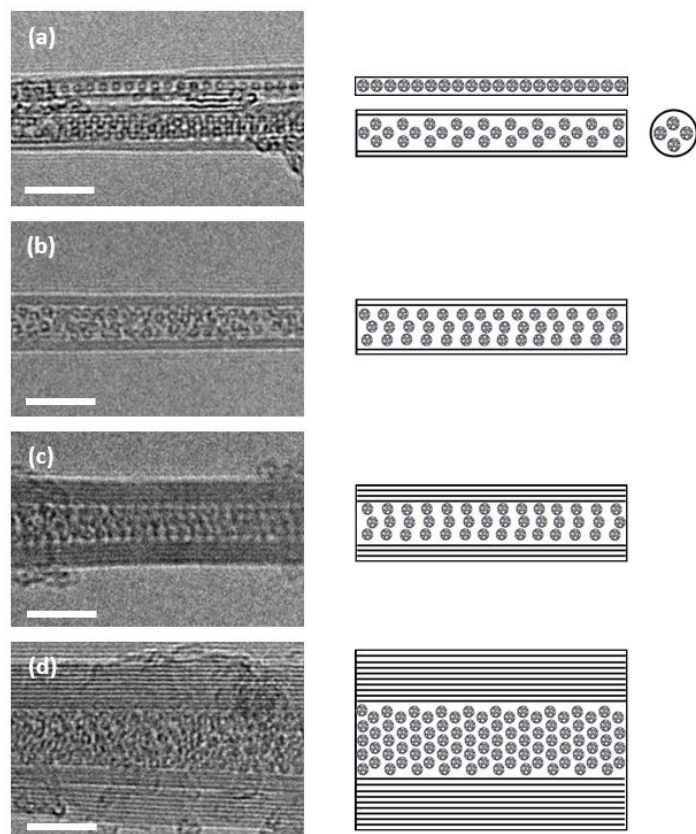

Figure 2. TEM images and schematic representations of C_{60}@BNNT demonstrating the dependence of the stacking arrangement of C_{60} on the internal diameter of the respective BNNT: (a) 1.2 nm (top), 2.1 nm (bottom), (b) 2.4-2.6 nm, (c) *ca*. 2.6 nm and (d) 4.4-5.2 nm. The stacking arrangements are assigned to (a) linear (top), two layer phase (bottom), (b) helical, (c) helical and (d) amorphous. The schematic representations indicate the possible stacking arrangements of C_{60} inside BNNTs of uniform diameter. Scale bars are 5 nm.

In wider BNNTs, fullerenes adjust their positions to maximise the interactions with the host-nanotube and to fill the cylindrical cavity in the most efficient way (Figure 2b, c and d and Supporting Information, Figure S5), which is analogous to the behaviour of C_{60} in wider CNTs.[12] This forms packing patterns of C_{60} which are clearly ordered in some cases (Figure

2a and c), but more disordered in others (Figure 2b and d). For example, there is no real packing order in the very large BNNT in Figure 2d possibly due to the wide, yet variable, diameter of BNNT in this instance. Figure 2c appears to show a corkscrew arrangement of C_{60} inside the BNNT with an internal diameter of 2.6 nm which agrees with previous studies of C_{60} in BNNTs,[37] but some other corkscrew packing patterns, such as in Figure 2b appear to be discontinuous along the length of the nanotube, possibly due to the non-uniform diameter of the host-BNNT. Non-helical packing patterns are also present (Figure 2a), such as the two-molecule layer phase inside a 2.1 nm diameter BNNT, narrower than that described for C_{60} inside a *ca.* 2.6 nm DWCNT.[12] Statistical analysis of multiple electron micrographs indicated that around 25% of the BNNTs are completely filled.

To further probe the efficiency of encapsulation of C_{60} in BNNTs, IR and UV-vis spectroscopies were performed (Figure 3). Being electrically insulating and optically transparent, BNNTs should allow the vibrations of guest-molecules to be directly analysed by IR spectroscopy, unlike CNTs that have often hindered such analysis.[56] Indeed, the IR spectrum of toluene-washed C_{60}@BNNT (Figure 3a) contains prominent bands at 803 and 1375 cm^{-1} corresponding to the out-of-plane radial buckling (R) mode and the in-plane stretching modes of h-BN in BNNTs respectively,[57, 58] as well as weak features at 527, 576 and 1183 cm^{-1} consistent with known vibrational modes of $T_{1u}(1)$, $T_{1u}(2)$ and $T_{1u}(3)$ symmetry in C_{60}.[59] Through correlation of the dependence of the absorbance intensity at 527 cm^{-1} ($T_{1u}(1)$) with the mass of C_{60} (Figure 3b and c), the quantity of C_{60} in C_{60}@BNNT was found to be *ca.* 29 mass%. Corresponding UV-vis spectroscopy analysis (Figure 3d, e and f) indicated that the amount of C_{60} extracted from C_{60}@BNNT through extensive sonication in toluene was *ca.* 37%. The slight differences in loading of C_{60} inside BNNTs obtained by different spectroscopic methods can be readily attributed to the wide distribution of BNNT diameters present within a given sample.
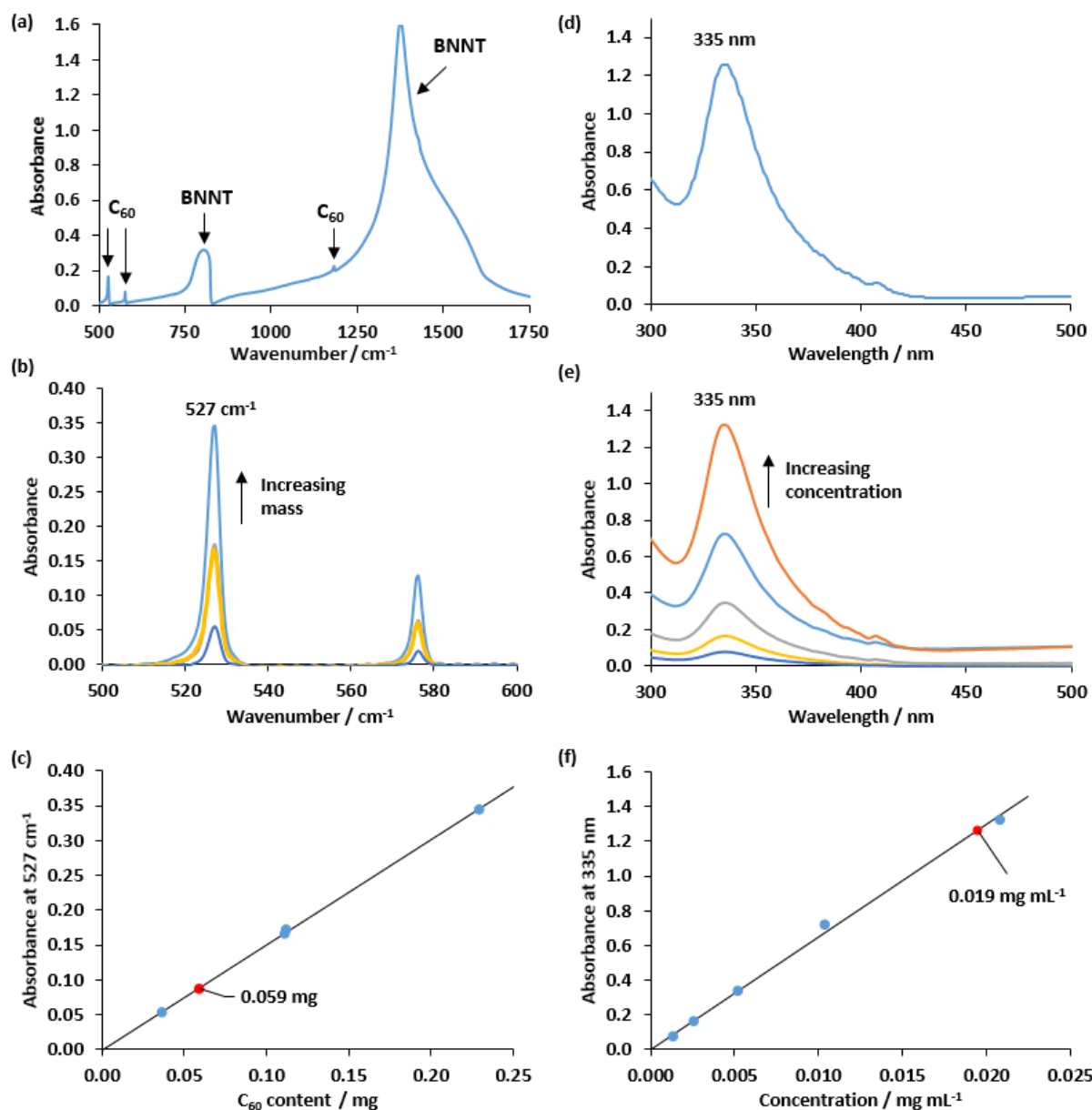
Figure 3. (a) IR spectrum of C_{60}@BNNT. (b) Baseline-corrected IR spectra of C_{60} with varying C_{60} content (0.036, 0.111, 0.112 and 0.230 mg) in potassium bromide (265 mg) used to construct the calibration curve (c) which correlates the intensity of the absorbance at 527 cm^{-1} ($T_{1u}(1)$) with C_{60} content. The amount of C_{60} in C_{60}@BNNT using this method was found to be 0.059 mg in 0.260 mg (mass ratio ca. 29%). $y=1.509x$, $R^2=1.000$, standard error = 0.01. (d) UV-vis spectrum of C_{60} extracted from C_{60}@BNNT through extensive sonication in toluene (4 mL). (e) UV-vis spectra of C_{60} at a variety of concentrations in toluene (0.0013, 0.0026, 0.0052, 0.0104 and 0.0208 mg mL^{-1}) used to produce the calibration curve (f) which

10

correlates the intensity of the absorbance at 335 nm with the concentration of C_{60} in toluene. The amount of C_{60} extracted from C_{60}@BNNT using this method was found to be 0.019 mg in 0.07 mg (mass ratio *ca.* 37%). $y=64.7x$, $R^2=0.998$, standard error=1.15.

It is important to note that both the IR spectroscopy method, where C_{60} remains within the internal channel of BNNTs during analysis, and the UV-vis spectroscopy approach, where C_{60} has been removed, gives approximately the same loading of C_{60} in BNNTs as was observed by TEM analysis. Moreover, comparison of the spectroscopy approaches confirms that C_{60} can be effectively removed from within BNNTs by excessive sonication in organic solvent (toluene), a feat that cannot be achieved from within CNTs. This suggests that the host-guest interactions in C_{60}@BNNT are likely to be weaker than in C_{60}@CNT; however, the poor host-guest fit (the van der Waals diameter of C_{60} of 1.0 nm is smaller than the mean internal diameter of BNNTs of 2.45±1.19 nm) precludes a large number of C_{60}-BNNT contacts and as such the encapsulated fullerenes can be solvated in a manner analogous to that observed in the bulk fcc-crystal. This observation also indicates that caution has to be exercised when purifying the products: repeated rinsing with toluene should be used for removing C_{60} molecules from the surface but sonication should be avoided as it results in emptying the BNNTs.

Temperature dependent IR spectroscopy was used to identify the different vibrational modes of guest-molecules of C_{60} inside BNNTs as orientational order develops with the lowering of the temperature (Figure 4).
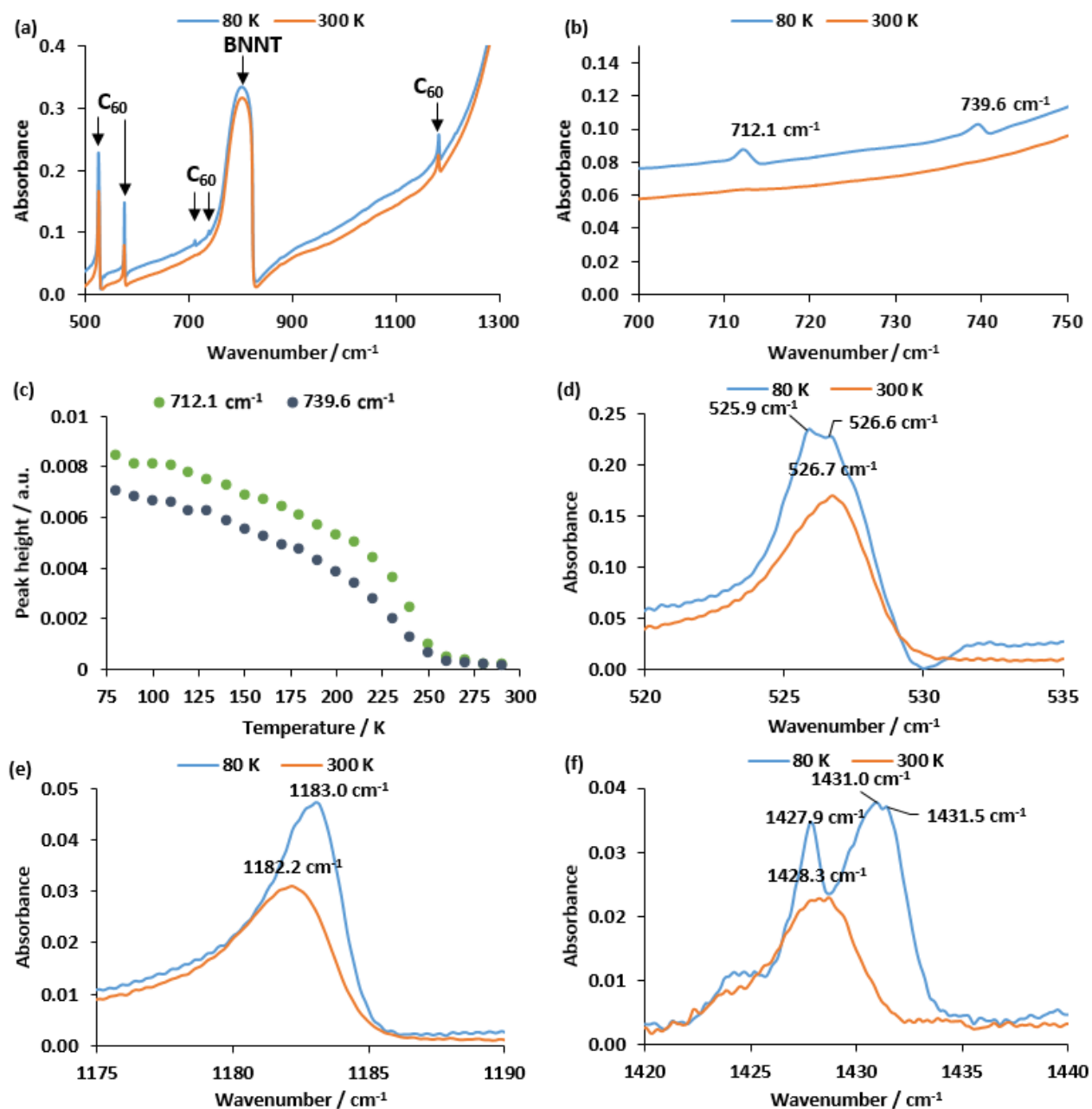
Figure 4. High resolution IR spectra of C_{60}@BNNT at 80 and 300 K in the range 500-1300 cm^{-1} (a) and 700-750 cm^{-1} (b). The height of the peaks at 712.1 and 739.6 cm^{-1} (H_u) vary as a function of temperature (c). The band at 526.7 cm^{-1} ($T_{1u}(1)$) increases in intensity and splits into two peaks at 525.9 and 526.6 cm^{-1} (d), the band intensity at 1182.2 cm^{-1} ($T_{1u}(3)$) increases and shifts to higher energy (e) and the band at 1428.3 cm^{-1} ($G_u/T_{1u}(4)$) splits into three bands when cooled from 300 K to 80 K (f).

At 300 K, the spectrum of C_{60} in C_{60}@BNNT contains only the four IR-active T_{1u} modes of the icosahedral C_{60} molecule. As the temperature decreases below the orientational phase transition temperature, the molecular rotation is restricted leading to a lowering of the symmetry as the molecules have to adjust to the crystal structure. This results in splitting of the triply degenerate T_{1u} modes and the appearance of previously IR-inactive new modes (Figure 4a). The new bands at 712.1 and 739.6 cm^{-1} (Figure 4b), assigned to H_u symmetry,[60] increase in intensity with decreasing temperature (Figure 4c). The temperature where they appear is around 250 K, exactly where the orientational phase transition occurs in fcc C_{60}.[54] Splitting of the T_{1u} modes, such as the 526.7 cm^{-1} band ($T_{1u}(1)$) becoming two at 525.9 cm^{-1} and 526.6 cm^{-1} (Figure 4d) and the 1428.3 cm^{-1} band ($G_u/T_{1u}(4)$) splitting into three bands at 1427.9, 1431.0 and 1431.5 cm^{-1} (Figure 4f), along with the lack of splitting of the $T_{1u}(3)$ mode (Figure 4e), are also consistent with earlier observations in the bulk fcc crystal.[59] This temperature-dependent behaviour suggests that C_{60} molecules are in a similar environment when encapsulated in the BNNTs. Vibrational spectroscopy, however, reflects short-range rather than long-range order: the lowering of symmetry indicates that the molecular rotation has stopped due to interaction with neighbouring fullerenes. The orientational transition temperature is determined by the intermolecular distance[61] rather than the long-range crystal structure; so long as the intermolecular distance is similar, these results can be reconciled with any arrangement shown in Figure 2.

The presence of C_{60} is also proven by Raman spectroscopy (see Supporting Information, Figure S6). Five of the ten Raman-active modes can be clearly identified in the Raman spectrum of C_{60}@BNNT.[62] We regard this as sufficient, as the remaining modes have small intensity. Encapsulation does not cause a measurable shift in the frequency of these vibrational modes, unlike what has been reported for narrow-diameter carbon nanotube

peapods.[63] However, such behaviour was observed in carbon nanotube peapods with a large mean diameter and a broad diameter distribution, similar to our BNNTs.[64]

The polymerisation and coalescence of guest C_{60} molecules into a CNT inside the host-BNNT offers an exciting opportunity to form a conducting nanowire inside an insulating BNNT. Previous attempts to fabricate CNT@BNNT have been made by other routes, such as the coating of CNT with boron nitride.[65-72] However, the formation of CNTs within pre-formed BNNTs would be more desirable because the structure of the outer insulating nanotube is well-defined and easier to control with uniform coverage of BN. Furthermore, this approach also permits the formation of very narrow SWCNTs in BNNTs, a nanostructure with favourable properties in chemical sensing.[73] Two noteworthy examples of forming CNT@BNNT using pre-formed BNNTs involve the electron irradiation of amorphous carbon[74] and C_{60}[37] inside BNNTs, though the inherent nature of this method is not scalable.

Previous studies on the thermal transformations of C_{60}@CNT suggest that confined C_{60} molecules begin to coalesce at ~800 ˚C inside a CNT[19] and at 1200 ˚C most of the C_{60} has rearranged to form an internal CNT within the host-CNT.[75] The templating effects of the host-CNT were shown to be important in the CNT formation, as the diameter of the inner CNT is dependent on the outer nanotube and completely independent of the size of C_{60}.[19] In our study, we heated C_{60}@BNNT at 1200 °C for 6 hr under argon to stimulate the polymerisation and coalescence processes, similar to those well-documented for C_{60}@CNT. The method was varied through several approaches (see Supporting Information, Table S1, Figure S9, S10 and S11), yet did not show any clear benefits. During the heating process, C_{60} desorbs from within the wider (>2 nm diameter) BNNTs, and as such CNTs are only formed in narrow BNNTs, consistent with the previously reported desorption of C_{60} from wider CNT.[75] Furthermore, TGA measurements in air of C_{60}@BNNT after heating at 1200 °C in

14

argon show a reduction in the carbon content of the material by a factor of four, from around 8% of C in C_{60}@BNNT before heating (see Supporting Information, Figure S7) to around 2% after (see Supporting Information, Figure S8). It is likely that larger nanotubes, with lower host-guest contact area and hence weaker van der Waals interactions between the fullerene and the BNNTs, cannot retain C_{60} inside the nanotube and as such some of the confined material becomes lost during heating.

The Raman spectrum of C_{60}@BNNT shows clear changes on thermal annealing (see Supporting Information, Figure S12): the C_{60} modes disappear and those of carbon nanotubes (the D and G mode at around 1300 and 1600 cm^{-1} respectively) are observed. The growth of inner nanotubes proves that the majority of C_{60} molecules were encapsulated.

TEM imaging of C_{60}@BNNT after heating reveals that most molecules have undergone coalescence to tubular structures with mean diameters of 1.1±0.2 nm and lengths of 4.3±2.9 nm, with a modal van der Waals separation of *ca*. 0.34 nm between the CNT and BNNT (Figure 5).
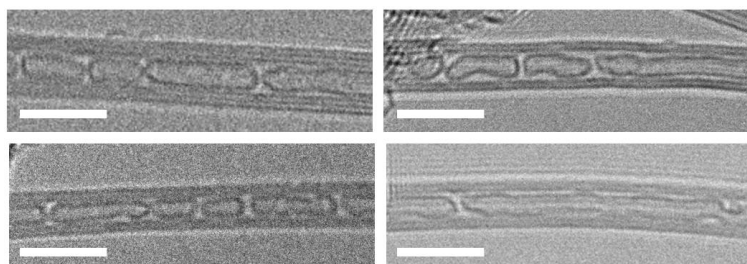

Figure 5. Bright field TEM images of CNT@BNNT formed from C_{60}@BNNT at 1200 °C. Scale bars are 5 nm.

To confirm that the cylindrical structures observed in the TEM images of CNT@BNNT are in fact carbon nanotubes encapsulated in boron nitride nanotubes, the sample was analysed by

electron energy loss spectroscopy (EELS) and energy-filtered TEM (EFTEM) imaging, which

maps the location of each element within this hybrid nanomaterial (Figure 6).
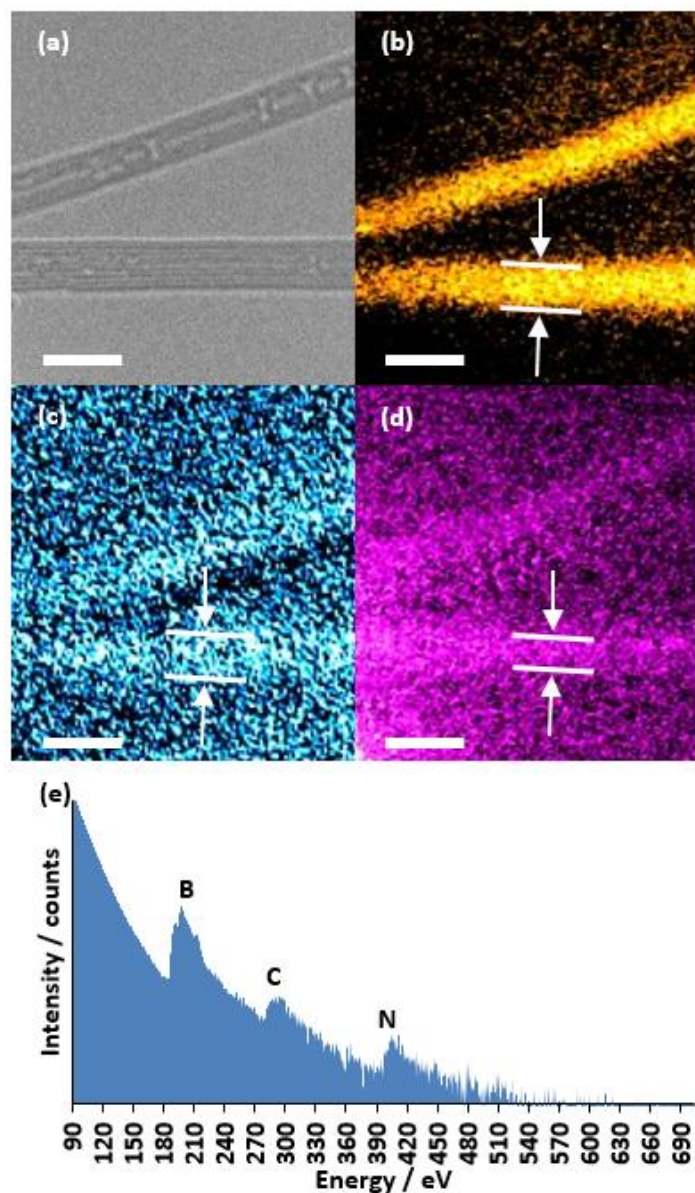

Figure 6. (a) Bright field TEM image of CNT@BNNT produced by heating C_{60}@BNNT. EELS EFTEM elemental maps showing the distributions of boron (b), nitrogen (c) and carbon (d) in the same nanotube. The line widths for boron, carbon and nitrogen are 3.9, 3.2 and 3.9 nm respectively. (e) A representative electron energy loss spectrum of CNT@BNNT. Scale bars are 5 nm.

16

The linear contrast showing the location of carbon in the CNT@BNNT structure is visibly narrower (3.2 nm) than those attained for boron (3.9 nm) and nitrogen (3.9 nm), providing further evidence that the structures are indeed CNTs embedded within BNNTs. Since BNNTs are electrical insulators, charge induced by the e-beam during TEM analysis builds up and cannot be removed from the sample. This causes the BNNTs to move around, thus blurring EFTEM images during the data acquisition, such as in the case of upper CNT@BNNT in Figure 6 which appears broader as a result. The bottom nanotube in Figure 6, however, is fixed firmly at both ends on the TEM grid, restricting the movement and producing clearer elemental maps. It is also worth noting that with B:N = 1:1, the nitrogen signal will appear much weaker than the boron signal, as the relationship between core-loss intensity and energy is approximately that of an inverse power law.[77]

UV-vis spectroscopy is used as a tool to understand the size of the electronic band gap of the new material CNT@BNNT (Figure 7).
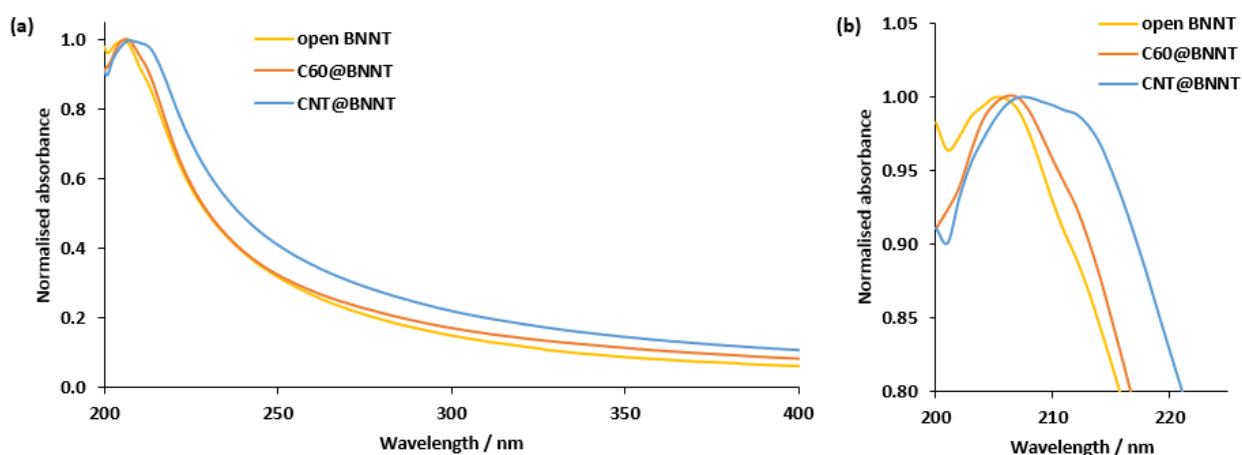

Figure 7. (a) UV-vis spectra of open and purified BNNTs, C_{60}@BNNT and CNT@BNNT. The experimentally determined band gaps are 6.04 eV (205.3 nm) for open and purified BNNTs, 6.00 eV (206.5 nm) for C_{60}@BNNT and 5.98 eV (207.4 nm) for CNT@BNNT. A

shoulder at 212 nm in the spectrum of CNT@BNNT (b) is consistent with the π-π^* absorption of a narrow SWCNT.

The absorption maximum shifts to a higher wavelength as the BNNT is opened and purified, filled with C_{60} and then finally transformed into CNT@BNNT. For CNT@BNNT, the electronic structures of the BNNTs and CNTs in the composite are predicted to change when compared to the pristine nanotube analogues due to the stretching of C-C bonds and compression of B-N bonds,[78] explaining our measured change in the band gap of BNNTs when the CNT is encapsulated. However, the BNNTs will remain insulating and the CNT core will be electronically conducting.[78] The most significant result from the UV-vis spectroscopy measurements is that the absorption band of CNT@BNNT is significantly broader than for any other samples and has a distinct shoulder at 212 nm (Figure 7b), which corresponds to the $\pi - \pi^*$ excitation of a single-walled carbon nanotube with a diameter of 0.90 nm.[79] This value is consistent with the diameter of a carbon nanotube formed from C_{60} inside BNNTs measured in TEM images of CNT@BNNT (0.9-1.2 nm at the widest point, with narrow parts of as small as 0.4 nm).

3. Conclusion

Boron nitride nanotubes have been demonstrated as effective nanoscale containers and reactors for molecules of fullerene C_{60} which can be inserted into BNNTs from the gas phase to form ordered quasi-one-dimensional arrays. The packing arrangement of fullerenes in C_{60}@BNNT was shown to be different to the packing of C_{60} in the bulk crystal and highly dependent on the internal diameter of the host-nanotube, but IR spectroscopy analysis of the guest-molecules suggest that the dynamic behaviour and temperature-controlled phase transitions of C_{60} in BNNTs are the same as in the bulk fullerene crystal. The thermal

treatment of C_{60}@BNNT at 1200 °C in argon triggers drastic transformations of the guest-molecule which polymerise and coalesce into carbon nanotubes inside boron nitride nanotubes thus forming a hybrid nanostructure CNT@BNNT, as confirmed by high resolution bright field TEM imaging and EELS EFTEM elemental mapping of individual CNT@BNNT structures, which suggests that B and N comprise the shell and C is located in the core of this hybrid nanostructure. Furthermore, UV-vis absorption spectroscopy indicates a new optical transition in CNT@BNNT material (absent in BNNTs or C_{60}@BNNT) suggesting that the average diameter of the guest carbon nanotube is ~0.9 nm which correlates well with that measured by TEM. Overall, the concentric structure CNT@BNNT with insulating BNNTs as the outer shell, and conducting CNTs as the inner core, represents an excellent candidate material for nanoscale coaxial cables which are required for several electronic and sensing applications.[39-41] Our method of carbon nanotube growth from molecules, directly inside BNNTs builds on the concept of nanoreactors we developed for carbon nanotubes, and provides the first scalable method for the controlled growth of conducting nanotubes inside insulating nanotubes.

4. Experimental Section

General experimental: All common reagents and solvents were purchased from Sigma-Aldrich, UK and used without further purification unless stated otherwise. Water was purified (> 18.0 MΩ cm) using a Barnstead NANOpure II system. TEM imaging was performed using a JEOL 2100F TEM (field emission gun source, information limit < 0.19 nm) at 100 kV at room temperature. EEL spectra were acquired using a Gatan Tridiem energy filter from regions defined by the selected area aperture to exclude any contribution from the supporting carbon film. Acquisition parameters were a 2 mm spectrometer aperture, with a dispersion of 0.3 eV/pixel. The line widths for boron, carbon and nitrogen in EELS EF-TEM elemental maps were determined by fitting the intensity profile in Digital Micrograph software. EDX

spectra were recorded using an Oxford Instruments 30mm^2 Si(Li) detector or an Oxford Instruments x-Max 80 SDD running on an INCA microanalysis system. Samples for TEM, EELS and EDX were typically prepared by casting several drops of a suspension of nanotubes onto copper-grid mounted "lacy" carbon films. Raman spectroscopy was conducted using a laser wavelength of 355 nm. FTIR spectroscopy was performed on a Bruker IFS66v spectrometer using the KBr pellet technique. UV-vis spectroscopy was performed using an Ocean Optics QE65000 spectrometer or Perkin-Elmer Lambda 25 UV-vis spectrometer. Thermogravimetric analysis (TGA) was performed using a TA Instruments SDT Q600 under a flow of air at a heating rate of 10 °C min^{-1} from room temperature to 1000 °C. Powder X-Ray diffraction measurements were performed on a PANalytical X'Pert PRO diffractometer equipped with a Cu Kα radiation source (λ = 1.5418 Å) in Bragg-Brentano geometry using a Si zero-background holder.

Opening BNNTs. To as-received BNNTs (100 mg, BNNT LLC, produced using the high temperature high pressure method) was added an aqueous solution of ammonium hydroxide (200 mL, 10 % in water) and the suspension homogenised by tip ultrasonication (20 kHz, 130 W Sonics Vibracell CPX150 ultrasonic processor) for 4, 10 or 24 hr at room temperature. Any visible clumps of BNNTs which had not dispersed were discarded. The resultant suspended grey/brown solid was collected by vacuum filtration (0.2 μm PTFE membrane) and washed with deionised water (20 mL). This was further heated at 800 °C for 1 hr, washed with hot (~90 °C) deionised water (~500 mL) and collected by vacuum filtration (0.2 μm PTFE membrane). Mass = 52 mg.

Filling BNNTs. Open and purified BNNTs (10 mg) and C$_{60}$-fullerene (10 mg, SES Research) were sealed under vacuum (10^{-5} mbar) in a Pyrex tube and heated at 600 °C for 20 hr. The solid was collected by vacuum filtration (0.2 μm PTFE membrane) and washed extensively with toluene until the filtrate became colourless. Mass = 8.2 mg.

Formation of CNT@BNNT. C_{60}@BNNT (9.0 mg) was sealed under Ar (0.7 bar) in a quartz ampoule and heated at 1200 ^{o}C for 6 h. Mass = 7.1 mg.

Supporting Information

Supporting Information is available from the Wiley Online Library or from the author.

References

[1]   M.-F. Yu, O. Lourie,, M. J. Dyer, K. Moloni, T. F. Kelly, R. S. Ruoff, *Science* **2000**, *287*, 637.

[2]   H. Dai, *Acc. Chem. Res.* **2002**, *35*, 1035.

[3]   J. W. G. Wilder, L. C. Venema, A. G. Rinzler, R. E. Smalley, C. Dekker, *Nature* **1998**, *391*, 59.

[4]   B. W. Smith, M. Monthioux, D. E. Luzzi, *Nature* **1998**, *396*, 323.

[5]   T. Okazaki, Y. Iizumi, S. Okubo, H. Kataura, Z. Liu, K. Suenaga, Y. Tahara, M. Yudasaka, S. Okada, S. Iijima, *Angew. Chem. Int. Ed.* **2011**, *50*, 4853.

[6]   B. Botka, M. E. Füstös, H. M. Tóháti, K. Németh, G. Klupp, Z. Szekrényes, D. Kocsis, M. Utczás, E. Székely, T. Váczi, G. Tarczay, R. Hackl, T. W. Chamberlain, A. N. Khlobystov, K. Kamarás, *Small* **2014**, *10*, 1369.

[7]   Y. K. Chen, A. Chu, J. Cook, M. L. H. Green, P. J. F. Harris, R. Heesom, M. Humphries, J. Sloan, S. C. Tsang, J. F. C. Turner, *J. Mater. Chem.* **1997**, *7*, 545.

[8]   P. M. Ajayan, T. W. Ebbesen, T. Ichihashi, S. Iijima, K. Tanigaki, H. Hiura, *Nature* **1993**, *362*, 522.

[9]   E. Dujardin, T. W. Ebbesen, H. Hiura, K. Tanigaki, *Science* **1994**, *265*, 1850.

[10]   J. Sloan, J. Hammer, M. Zwiefka-Sibley, M. L. H. Green, *Chem. Commun.* **1998**, 347.

[11]   Y. J. Dappe, *J. Phys. D Appl. Phys.* **2014**, *47*, 083001.

[12]   A. N. Khlobystov, D. A. Britz, A. Ardavan, G. A. D. Briggs, *Phys. Rev. Lett.* **2004**, *92*, 245507.

[13]   D. A. Britz, A. N. Khlobystov, K. Porfyrakis, A. Ardavan, G. A. D. Briggs, *Chem. Commun.* **2005**, 37.

[14]   A. Botos, J. Biskupek, T. W. Chamberlain, G. A. Rance, C. T. Stoppiello, J. Sloan, Z. Liu, K. Suenaga, U. Kaiser, A. N. Khlobystov, *J. Am. Chem. Soc.* **2016**, *138*, 8175.

[15]   V. V. Chaban, O. V. Prezhdo, *ACS Nano* **2011**, *5*, 5647.

[16]   S. Campestrini, C. Corvaja, M. De Nardi, C. Ducati, L. Franco, M. Maggini, M. Meneghetti, E. Menna, G. Ruaro, *Small* **2008**, *4*, 350.

[17]   H. E. Lim, Y. Miyata, R. Kitaura, Y. Nishimura, Y. Nishimoto, S. Irle, J. H. Warner, H. Kataura, H. Shinohara, *Nature Commun.* **2013**, *4*, 2548.

[18] Y. Nakanishi, H. Omachi, N. A. Fokina, P. R. Schreiner, R. Kitaura, J. E. P. Dahl, R. M. K. Carlson, H. Shinohara, *Angew. Chem. Int. Ed.* **2015**, *54*, 10802.

[19] S. Bandow, M. Takizawa, K. Hirahara, M. Yudasaka, S. Iijima, *Chem. Phys. Lett.* **2001**, *337*, 48.

[20] G. Pagona, G. Rotas, A. N. Khlobystov, T. W. Chamberlain, K. Porfyrakis, N. Tagmatarchis, *J. Am. Chem. Soc.* **2008**, *130*, 6062.

[21] C. S. Allen, Y. Ito, A. W. Robertson, H. Shinohara, J. H. Warner, *ACS Nano* **2011**, *5*, 10084.

[22] A. Chuvilin, E. Bichoutskaia, M. C. Gimenez-Lopez, T. W. Chamberlain, G. A. Rance, N. Kuganathan, J. Biskupek, U. Kaiser, A. N. Khlobystov, *Nature Mater.* **2011**, *10*, 687.

[23] A. V. Talyzin, I. V. Anoshkin, A. V. Krasheninnikov, R. M. Nieminen, A. G. Nasibulin, H. Jiang, E. I. Kauppinen, *Nano Lett.* **2011**, *11*, 4352.

[24] A. I. Chernov, P. V. Fedotov, A. V. Talyzin, I. S. Lopez, I. V. Anoshkin, A. G. Nasibulin, E. I. Kauppinen, E. D. Obraztsova, *ACS Nano* **2013**, *7*, 6346.

[25] H. M. Ghassemi, R. S. Yassar, *Appl. Mech. Rev.* **2010**, *63*, 020804.

[26] Y. Chen, J. Zou, S. J. Campbell, G. Le Caer, *Appl. Phys. Lett.* **2004**, *84*, 2430.

[27] X. Blase, A. Rubio, S. G. Louie, M. L. Cohen, *Europhys. Lett.* **1994**, *28*, 335.

[28] M. Terrones, J. M. Romo-Herrera, E. Cruz-Silva, F. Lopez-Urias, E. Munoz-Sandoval, J. J. Velazquez-Salazar, H. Terrones, Y. Bando, D. Golberg, *Mater. Today* **2007**, *10*, 30.

[29] D. Golberg, Y. Bando, M. Mitome, K. Fushimi, C. Tang, *Acta Mater.* **2004**, *52*, 3295.

[30] W. Han, P. Redlich, F. Ernst, M. Ruhle, *Appl. Phys. Lett.* **1999**, *75*, 1875.

[31] W.-Q. Han, A. Zettl, *Appl. Phys. Lett.* **2002**, *81*, 5051.

[32] Y. Bando, K. Ogawa, D. Golberg, *Chem. Phys. Lett.* **2001**, *347*, 349.

[33] F.-F. Xu, Y. Bando, D. Golberg, M. Hasegawa, M. Mitome, *Acta Mater.* **2004**, *52*, 601.

[34] D. Golberg, F.-F. Xu, Y. Bando, *Appl. Phys. A* **2003**, *76*, 479.

[35] W.-Q. Han, C. W. Chang, A. Zettl, *Nano Lett.* **2004**, *4*, 1355.

[36] T. Pham, A. Fathalizadeh, B. Shevitski, S. Turner, S. Aloni, A. Zettl, *Nano Lett.* **2016**, *16*, 320.

[37] W. Mickelson, S. Aloni, W.-Q. Han, A. Zettl, *Science* **2003**, *300*, 467.

[38] J. W. Kang, H. J. Hwang, *J. Phys. Condens. Matter* **2004**, *16*, 3901.

[39] J. Wang, C. H. Lee, Y. K. Yap, *Nanoscale* **2010**, *2*, 2028.

[40] P. Singla, N. Goel, V. Kumar, S. Singhal, *Ceram. Int.* **2015**, *41*, 10565.

[41] Q. Weng, X. Wang, X. Wang, Y. Bando, D. Golberg, *Chem. Soc. Rev.* **2016**, *45*, 3989.

[42] Y. Liao, Z. Chen, J. W. Connell, C. C. Fay, C. Park, J.-W. Kim, Y. Lin, *Adv. Funct. Mater.* **2014**, *24*, 4497.

[43] C. H. Lee, D. Zhang, Y. P. Yap, *J. Phys. Chem. C* **2012**, *116*, 1798.

[44] C. Zhi, N. Hanagata, Y. Bando, D. Golberg, *Chem. Asian J.* **2011**, *6*, 2530.

[45] H. Chen, Y. Chen, J. Yu, J. S. Williams, *Chem. Phys. Lett.* **2006**, *425*, 315.

[46] D. Golberg, Y. Bando, Y. Huang, T. Terao, M. Mitome, C. Tang, C. Zhi, *ACS Nano* **2010**, *4*, 2979.

[47] D. Golberg, Y. Bando, C. C. Tang, C. Y. Zhi, *Adv. Mater.* **2007**, *19*, 2413.

[48] P. Kondratyuk, J. T. Yates, *J. Am. Chem. Soc.* **2007**, *129*, 8736.

[49] L. A. Girifalco, M. Hodak, R. S. Lee, *Phys. Rev. B* **2000**, *62*, 13104.

[50] H. Ulbricht, G. Moos, T. Hertel, *Phys. Rev. Lett.* **2003**, *90*, 095501.

[51] K. S. Troche, V. R. Coluci, S. F. Braga, D. D. Chinellato, F. Sato, S. B. Legoas, R. Rurali, D. S. Galvao, *Nano Lett.* **2005**, *5*, 349.

[52] J. H. Warner, Y. Ito, M. Zaka, L. Ge, T. Akachi, H. Okimoto, K. Porfyrakis, A. A. R. Watt, H. Shinohara, G. A. D. Briggs, *Nano Lett.* **2008**, *8*, 2328.

[53] K. Berland, P. Hyldgaard, *Phys. Rev. B* **2013**, *87*, 205421.

[54]   P. A. Heiney, J. E. Fischer, A. R. McGhie, W. J. Romanow, A. M. Denenstein, J. P. McCauley, A. B. Smith, D. E. Cox, *Phys. Rev. Lett.* **1991**, *66*, 2911.

[55]   P. A. Heiney, *J. Phys. Chem. Solids* **1992**, *53*, 1333.

[56]   Á. Pekker, G. Németh, A. Botos, H. M. Tóháti, F. Borondics, Z. Osváth, L. P. Biró, K. Walker, A. N. Khlobystov, K. Kamarás, *Phys. Status Solidi B* **2016**, *253*, 2457.

[57]   B. Fakrach, A. Rahmani, H. Chadli, K. Sbai, M. Bentaleb, J.-L. Bantignies, J.-L. Sauvajol, *Phys. Rev. B* **2012**, *85*, 115437.

[58]   C. H. Lee, M. Xie, V. Kayastha, J. Wang, Y. K. Yap, *Chem. Mater.* **2010**, *22*, 1782.

[59]   K. Kamarás, L. Akselrod, S. Roth, A. Mittelbach, W. Hönle, H.G. von Schnering, *Chem. Phys. Lett.* **1993**, *214*, 338.

[60]   R. A. Jishi, R. M. Mirie, M. S. Dresselhaus, *Phys. Rev. B* **1992**, *45*, 13685.

[61]   S. Pekker, É. Kováts, G. Oszlányi, G. Bényei, G. Klupp, G. Bortel, I. Jalsovszky, E. Jakab, F. Borondics, K. Kamarás, M. Bokor, G. Kriza, K. Tompa, G. Faigel, *Nature Mater.* **2005**, *4*, 764.

[62]   D. S. Bethune, G. Meijer, W. C. Tang, H. J. Rosen, W. G. Golden, H. Seki, C. A. Brown, M. S. de Vries, *Chem. Phys. Lett.* **1991**, *179*, 181.

[63]   R. Pfeiffer, H. Kuzmany, T. Pichler, H. Kataura, Y. Achiba, M. Melle-Franco, F. Zerbetto, *Phys. Rev. B* **2004**, *69*, 035404.

[64]   F. Simon, H. Peterlik, R. Pfeiffer, J. Bernardi, H. Kuzmany, *Chem. Phys. Lett.* **2007**, *445*, 288.

[65]   L. Jing, R. Y. Tay, H. Li, S. H. Tsang, J. Huang, D. Tan, B. Zhang, E. H. T. Teo, A. I. Y. Tok, *Nanoscale* **2016**, *8*, 11114.

[66]   C. Y. Su, Z. Y. Juang, Y. L. Chen, K. C. Leou, C. H. Tsai, *Diamond Relat. Mater.* **2007**, *16*, 1393.

[67]   Y. Morihisa, C. Kimura, M. Yukawa, H. Aoki, T. Kobayashi, S. Hayashi, S. Akita, Y. Nakayama, T. Sugino, *J. Vac. Sci. Technol. B* **2008**, *26*, 872.

[68] M. Mohai, I. Mohai, Z. Sebestyén, A. Gergely, P. Németh, J. Szépvölgyi, *Surf. Interface Anal.* **2010**, *42*, 1148.

[69] Y. J. Jeong, M. F. Islam, *Nanoscale* **2015**, *7*, 12888.

[70] X. Yang, Z. Li, F. He, M. Liu, B. Bai, W. Liu, X. Qiu, H. Zhou, C. Li, Q. Dai, *Small* **2015**, *11*, 3710.

[71] W.-L. Wang, J.-Q. Bi, W.-X. Sun, H.-L. Zhu, J.-J. Xu, M.-T. Zhao, Y.-J. Bai, *Mater. Chem. Phys.* **2010**, *122*, 129.

[72] L. Chen, H. Ye, Y. Gogotsi, *J. Am. Ceram. Soc.* **2004**, *87*, 147.

[73] D. R. Kauffman, A. Star, *Angew. Chem. Int. Ed.* **2008**, *47*, 6550.

[74] R. Arenal, A. Lopez-Bezanilla, *ACS Nano* **2014**, *8*, 8419.

[75] B. W. Smith, D. E. Luzzi, *Chem. Phys. Lett.* **2000**, *321*, 169.

[76] R. Pfeiffer, M. Holzweber, H. Peterlik, H. Kuzmany, Z. Liu, K. Suenaga, H. Kataura, *Nano Lett.* **2007**, *7*, 2428.

[77] R. F. Egerton, *Rep. Prog. Phys.* **2009**, *72*, 016502.

[78] Z. Zhang, W. Guo, G. Tai, *Appl. Phys. Lett.* **2007**, *90*, 133103.

[79] G. A. Rance, D. H. Marsh, R. J. Nicholas, A. N. Khlobystov, *Chem. Phys. Lett.* **2010**, *493*, 19.

A new route towards the preparation of the world's smallest co-axial cable, comprising an electrically conducting carbon nanotube inside an insulating boron nitride nanotube, is described utilizing the selective confinement and thermally-initiated transformation of molecules of C_{60}-fullerene inside boron nitride nanotube nanoreactors.

Keyword Nanoreactors

Kate E. Walker, Graham A. Rance,* Áron Pekker, Hajnalka M. Tóháti, Michael W. Fay, Rhys W. Lodge, Craig T. Stoppiello, Katalin Kamarás, Andrei N. Khlobystov*

Growth of carbon nanotubes inside boron nitride nanotubes by coalescence of fullerenes: towards the world's smallest co-axial cable

ToC figure

BNNT

C_{60}@BNNT

CNT@BNNT

a nanoscale coaxial cable